CrossMark

J. Fluid Mech. (2016), *vol.* 788, *pp.* 358–380. © Cambridge University Press 2016
doi:10.1017/jfm.2015.670

Jet-noise control by fluidic injection from a rotating plug: linear and nonlinear sound-source mechanisms

Maxime Kœnig[1,†], Kenzo Sasaki[2], André V. G. Cavalieri[2], Peter Jordan[3] and Yves Gervais[3]

[1]Acoustics Department, Safran Snecma, 77550 Moissy-Cramayel, France

[2]Instituto Tecnológico de Aeronáutica, São José dos Campos 12228900, Brazil

[3]Departement Fluides, Thermique, Combustion, Institut Pprime, 86036 Poitiers, France

(Received 27 January 2015; revised 27 August 2015; accepted 8 November 2015;
first published online 5 January 2016)

We present a study of the turbulent and acoustic fields of subsonic jets, controlled by means of a novel actuator that introduces perturbations via steady-fluidic actuation from a rotating centrebody. The actuation can produce louder or quieter jets, and these are analysed using time-resolved stereoscopic particle image velocimetry and a hot-wire anemometer. We place the analysis in the framework of wavepackets and linear stability theory, whence we show, using solutions of the linear parabolised stability equations, that the quieter flows can be understood to result from a mean-flow deformation that modifies wavepacket dynamics, and in particular their phase velocities, which are significantly reduced. The mean-flow deformation is shown, by a triple decomposition, to be due to the generation of Reynolds stresses associated with incoherent turbulence (rather than coherent structures) which arises when the actuation energises the flow with a frequency–azimuthal wavenumber (ω–m) combination to which the mean flow is stable. When the actuation excites the flow with an ω–m combination to which the mean flow is unstable, the response is dominated by coherent structures, whose rapid growth takes them beyond the linear limit, where they undergo quadratic wave interactions and lead, consequently, to a louder flow.

Key words: aeroacoustics, jet noise, noise control

1. Introduction

We know that jet noise can be manipulated, enhanced or reduced, through a modification of the flow conditions in the vicinity of the nozzle exit. The modification may be due to a change in the geometry of the nozzle, using tabs or chevrons for instance (Zaman, Bridges & Huff 2011) or non-circular nozzles (Gutmark & Grinstein 1999). It may result from the addition of mass and momentum via steady-fluidic injection (Henderson 2010). However, the synthesis, and/or 'optimisation', of noise-reduction strategies remains problematic, being either guided by trial and

† Email address for correspondence: maxime.koenig@snecma.fr

https://doi.org/10.1017/jfm.2015.670 Published online by Cambridge University Press

error or based on the laborious exploration of hopelessly large parameter spaces. In the latter scenario, partial automation may sometimes be possible (Maury *et al.* 2012).

The limited success of noise-control strategies can be attributed to the lack of a solid conceptual framework connecting perturbations near the nozzle to the sound energy radiated to the far field, one that would enable a clear interpretation of the control effect, and thereby provide physics-based guidance through the myriad actuation possibilities.

Were it not for the fact that we know turbulent shear flows to comprise an underlying order, so-called 'coherent structures', or wavepackets, the establishment of such a connection would appear unimaginable. New numerical algorithms based on the iterative, forward and backward, solution of the Navier–Stokes equations and their adjoint do allow the sensitivity of the radiated sound to changes in the nozzle region to be established and exploited for control (Freund 2001; Wei & Freund 2006; Kim *et al.* 2009). However, the cost of such computations is enormous, and their capacity to provide clear physical insight is confounded by the fact that the said connection is made through, and indeed hidden by, the chaotic motions of turbulence.

Wavepacket theory, the basis for which was laid in the 1960s and 1970s, is a simpler and yet pertinent means by which to establish a nozzle-to-sound connection that would guide jet-noise control. We here provide a very brief overview (for a more detailed treatment the reader is referred to the recent review of Jordan & Colonius (2013)), as this motivates the analysis methodology we pursue.

Following the observations of Mollo-Christensen (1963, 1967), a large body of experimental, theoretical and more recently numerical work has been dedicated to the eduction of wavepackets from turbulence (Crow & Champagne 1971; Lau, Fisher & Fuchs 1972; Hussain & Zaman 1981; Kerhervé *et al.* 2012), to their study as a sound-generation mechanism (Michalke 1970; Crow 1972; Crighton 1975; Michalke & Fuchs 1975; Ffowcs-Williams & Kempton 1978; Crighton & Huerre 1990; Sandham, Morfey & Hu 2006; Cavalieri *et al.* 2011*a*, 2012*b*; Kerhervé *et al.* 2012) and to their dynamic modelling (Michalke 1971; Liu 1974; Crighton & Gaster 1976; Tam & Morris 1980; Mankbadi & Liu 1984). Eduction methodologies (e.g. Kerhervé *et al.* 2012) demonstrate the existence of low-amplitude organised motions, coherent over space and time extents that far exceed the integral scales of turbulence. Sound-source modelling confirms the assertion by Mollo-Christensen (1963) that these motions can generate a directive sound field – superdirective according to Crighton & Huerre (1990) and validated experimentally by Cavalieri *et al.* (2012*a*) – due to an antenna effect (mutual interference between structures within the wavepacket). Modelling strategies, which have only recently been validated in a comprehensive manner (Gudmundsson & Colonius 2011; Cavalieri *et al.* 2012*a*; Rodrıguez *et al.* 2013), show that these motions are synonymous with linear hydrodynamic instabilities of the turbulent mean flow. The scale separation between wavepacket motions and random background turbulence justifies such a use of the mean flow (Crighton & Gaster 1976); the low fluctuation amplitude of wavepackets justifies the linearisation.

In unforced high-Reynolds-number turbulent jets, wavepackets are driven by in-flow perturbations associated with the nozzle boundary layer. The broadband character of these perturbations makes it difficult to establish a link between in-flow conditions and wavepacket evolution. The turbulent boundary layer is dominated by eddies of high azimuthal wavenumber that evolve into shear-layer turbulence of similar azimuthal structure. However, some small part of this structure drives low-order azimuthal modes in the jet; in addition to this azimuthal organisation, wavepackets are characterised by

https://doi.org/10.1017/jfm.2015.670 Published online by Cambridge University Press

distinctive axial and radial organisations, and at any given axial location a specific preferred frequency can be observed in the spectrum (this is most clearly visible in the potential core and in the evanescent near pressure field). However, these wavepackets are clearly not harmonic, being driven by in-flow motions whose phase is stochastic.

Unsteady periodic actuation, on the other hand, produced for instance by fluidic pulsing (Maury *et al.* 2009), plasma discharge (Samimy *et al.* 2007) or piezoelectric flapping (Butler & Calkins 2003), is a means by which perturbations may be imposed in a more controlled fashion at the nozzle: a well-defined frequency (i.e. with deterministic phase) and azimuthal mode combination can be introduced and the response of the flow (turbulence and sound) assessed with that knowledge. This is in contrast to the aforementioned steady-fluidic techniques, where the frequency–wavenumber structure of the near-nozzle perturbation is largely governed by the turbulence that results from the interaction between the main jet and the injected fluid.

In jets subjected to such harmonic in-flow forcing, wavepackets of different kinds may be present. The turbulent boundary layer continues to seed the flow with perturbations similar to the unforced case (provided that the actuation is such that the boundary-layer structure is not significantly modified), and so non-harmonic wavepackets similar to those of the unforced flow are possible; these will of course evolve differently if the mean flow of the forced flow differs from that of the unforced case. If the actuation is such that its (harmonic) frequency–azimuthal mode structure corresponds to an unstable shear-layer mode, harmonic wavepackets will arise and evolve with (superposed on) the stochastic wavepackets. In the case where actuation produces both harmonic and stochastic disturbances with frequency–wavenumber content to which the flow is unstable, harmonically and stochastically forced wavepackets will arise, in addition to the stochastic wavepackets driven by the boundary layer. The stochastic wavepackets due respectively to the boundary layer and the stochastic component of the forcing will, *a priori*, be indistinguishable; the harmonic wavepackets will, however, be identifiable due to their deterministic phase, and this fact will be exploited later in the paper.

A final component of the actuated flow that will be of importance in what follows is the turbulent response to actuation. Unsteadiness introduced by actuation, be it harmonic or otherwise, that has a frequency–wavenumber structure to which the flow is stable, will provoke the generation of turbulence not present in the unactuated flow. This turbulence will deform the mean flow, and thus modify the evolution of all wavepackets in the flow. This is a key idea in the analysis to follow.

In this sense, besides their practical interest, noise-controlled flows produced by unsteady actuation, be they louder or quieter, provide a useful setting for the testing of conceptual frameworks that would link actuation to sound. In this paper we present a novel actuator that produces an unsteady-fluidic perturbation in the near-nozzle region of a round jet. Depending on the frequency–wavenumber structure of the perturbation, the actuator can produce louder or quieter jets with respect to the baseline. The main contribution of this study is a rather complete analysis and interpretation of both control effects in terms of wavepacket theory.

The experiment and analysis methodology involve the introduction of perturbations dominated by azimuthal mode $m = 2$, over a range of frequencies, and a subsequent investigation of the response of the jet via triple decomposition of the velocity field. This permits eduction of the turbulence and phase-locked wavepacket components of the flow response as a function of actuation frequency. We then study the linear stability characteristics of the mean flows, the linear parabolised stability equations

https://doi.org/10.1017/jfm.2015.670 Published online by Cambridge University Press

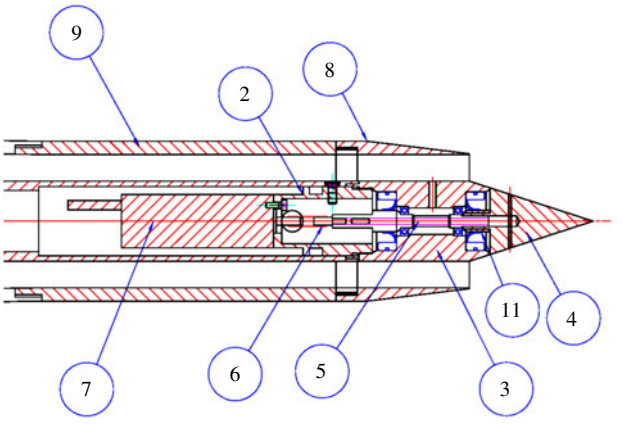


FIGURE 1. (Colour online) Sketch of the rotating plug mechanism, with the following parts highlighted: centreplug support (2), rolling bearing support (3), conical plug in PVC (4), crankshaft (5), heat shrink sleeve (6), Faulhaber 2057B electric motor (7), removable downstream nozzle (8), upstream nozzle (9) and seal (11).

(PSE) being used to account for the slow divergence of the jets. The analysis is focused on azimuthal modes $m = 0$ and $m = 2$. The former provides insight regarding changes in sound-source activity, while the latter is the key to understanding the control mechanism. A phenomenological interpretation of the controlled flows is thus proposed: actuation with an ω–m organisation to which the mean flow is stable leads to the generation of a turbulence whose Reynolds stresses deform the mean flow such that the dynamics of the most acoustically efficient wavepackets are advantageously modified. This interpretational framework was first proposed by Gudmundsson & Colonius (2007) and has subsequently been used by Sinha *et al.* to explain the effects of a different kind of fluidic actuator on the dynamics and sound-source mechanisms of turbulent jets; a significant reduction in phase velocity is identified as one of the decisive effects. A louder jet results when the flow is driven with an ω–m structure to which the mean flow is unstable; in this case, nonlinear (quadratic) wavepacket interactions become relevant and increase the radiated sound.

This paper is organised as follows. In § 2 the experimental apparatus is presented and the measurement methodologies are outlined. Section 3.1 contains a description of the acoustic response of the flow to actuation. The main aerodynamic changes produced are described in § 3.2, and a more complete analysis of these and the acoustic results, with respect to the sound-source mechanisms, is performed in § 4, supported by PSE solutions. Some conclusions and perspectives are given in § 5.

2. Experimental set-up

The experiments were performed at the PPRIME Institute anechoic jet-noise facility, Bruit et Vent, at the CEAT, Poitiers, France. An isothermal jet issuing from a round nozzle with a plug is studied. The exit Mach number is varied from 0.3 to 0.6, but on account of limitations in the rotation speeds possible with the actuator, the main results reported here are for the $M = 0.3$ case.

The nozzle and actuator are presented in figure 1. The main nozzle diameter is $D_{jet} = 0.05$ m; the actuator consists of a conical plug (centrebody) of diameter $D_{plug} = 0.03$ m and length $L_{plug} = 0.046$ m, mounted in the centre of the jet (see figure 2),

https://doi.org/10.1017/jfm.2015.670 Published online by Cambridge University Press

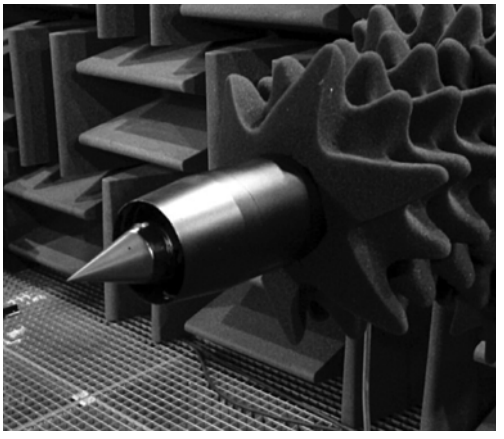


FIGURE 2. Rotating plug actuator in 'Bruit et Vent'.

and is driven in rotation by an electric motor. The air is ejected at 240 m s^{-1} into the main jet by two diametrically opposed control ports of 0.0013 m diameter. The control-jet flow rate is less than 0.5 % of that of the main jet. This value is relatively low compared with those of other fluidic injection studies aimed at jet-noise reduction (see Henderson (2010) for an exhaustive list), particularly for a turbulent jet. The study of the effects of different flow rates is currently an ongoing project by this group, and it will be important if the actuator proves to be effective at higher Mach numbers, which would make it viable for industrial applications. An attempt to ascertain how plug rotation alone, without fluidic injection, influences sound radiation was attempted; however, no broadband effect was seen in the acoustic field. This is consistent with the fact that, for the rotation speeds considered, the jet does not correspond to one with significant swirl (Kœnig 2011).

An equivalent diameter, D, is defined as

$$D = \sqrt{D_{jet}^2 - D_{plug}^2} = 0.04 \text{ m}. \tag{2.1}$$

This diameter is used as the reference length of the flow and gives a Reynolds number of $Re_D = U_j D/\nu = 2.7 \times 10^5$. The area contraction of the nozzle is 31. This convergent section is followed by a straight annular section of 150 mm length. A boundary-layer trip was used to force transition to turbulence 135 mm upstream of the nozzle exit. No boundary-layer trip was placed on the plug support. Hot-wire measurements were performed to measure velocities in the jet exit plane. Results for the mean and r.m.s. profiles are shown in figure 3. The boundary-layer characteristics obtained are typical of a turbulent case (Bridges & Hussain 1987; Cavalieri *et al.* 2013).

Microphone measurements were made at 30D from the jet, at downstream polar angles of 20° and 30°. For these shallow angles most of the acoustic radiation is related to wavepackets in the jet (Jordan & Colonius 2013). A moving average was used to smooth the spectra, and peaks associated with sound radiated by the electric motor have been removed by a notch filter in the results presented here. Measurement of the broadband baseline spectra showed a repeatability with less than 0.5 dB deviation for experiments performed with a six-month time separation.

https://doi.org/10.1017/jfm.2015.670 Published online by Cambridge University Press

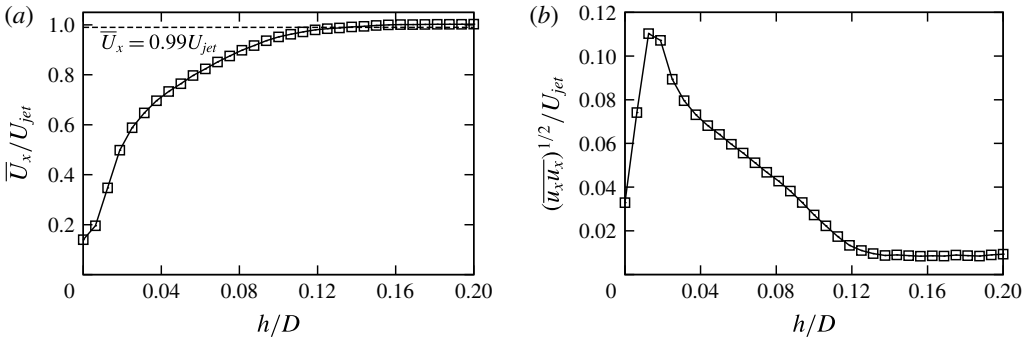


FIGURE 3. Boundary-layer profiles at the nozzle exit for a Mach 0.3 jet: (*a*) mean velocity; (*b*) r.m.s. value.

Velocity measurements were made using a LaVision time-resolved stereoscopic particle image velocimetry (hereafter TR-PIV) system and cameras with 1024 pixel × 1024 pixel resolution. The light source was a 10 mJ Quantronix Darwin duo laser (light sheet thickness 2 mm) and the flow was seeded with oil smoke. Three components of velocity were measured in r–θ planes at a range of axial stations by two SA1 Photron cameras. The sampling frequency was 2.7 kHz. Ten thousand PIV image pairs were recorded, this being sufficient for convergence of first- and second-order statistical moments. Image processing consisted of a five-pass correlation routine with 64 pixel × 64 pixel correlation for the first pass, 16 pixel × 16 pixel for the final pass and with a 50 % correlation overlap at each pass. The spatial resolution was one velocity vector every 0.75 mm for the small window size (near the jet exit) and one velocity vector every 1.5 mm for the large window size (around the end of the potential core). Hot-wire measurements are also presented in this paper to study the mixing layer close to the plug extremity where it was not possible to obtain accurate PIV measurements due to the proximity of the nozzle and plug surfaces. We use a single hot wire (2.5 μm), sampled at 250 kHz. An *in situ* calibration of the hot wire is performed as in Tutkun *et al.* (2009). The velocity is measured by the hot wire in x–r planes.

Due to the specificity of the actuator (unsteadiness introduced by rotation), the time-periodic disturbances are similar to those induced by a two-blade helix. Since the two microjets are nearly identical, the perturbation introduced by the actuator is dominated by an azimuthal mode 2, and by a microjet-passing frequency equal to twice the rotation frequency: $f_p = 2f_{rotation}$; we use this microjet-passing frequency to define a perturbation Strouhal number, $St_p = f_p D/U_j$.

3. Control effects

3.1. *In the sound field*

The injection flow rate and plug rotation frequency are the two control parameters. These were assessed for different main-jet Mach numbers, and the analysis indicates that, while similar noise reductions are probable at higher Mach numbers, the rotation-frequency limit (beyond a certain rotation speed the device overheats due to friction between the various moving parts) constrains us to study a Mach 0.3 jet. We therefore focus on this jet, at a fixed injection flow rate, and we explore the acoustic response

https://doi.org/10.1017/jfm.2015.670 Published online by Cambridge University Press

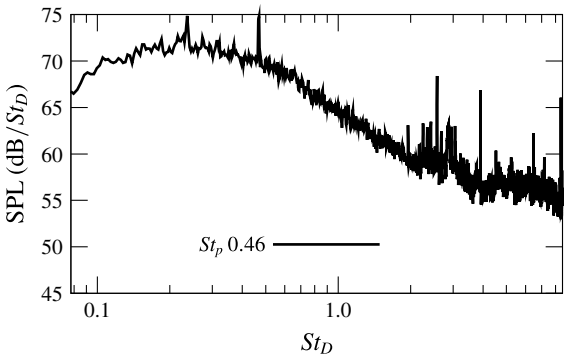


FIGURE 4. Acoustic spectrum prior to the filtering, for the $St_p = 0.46$ controlled jet.

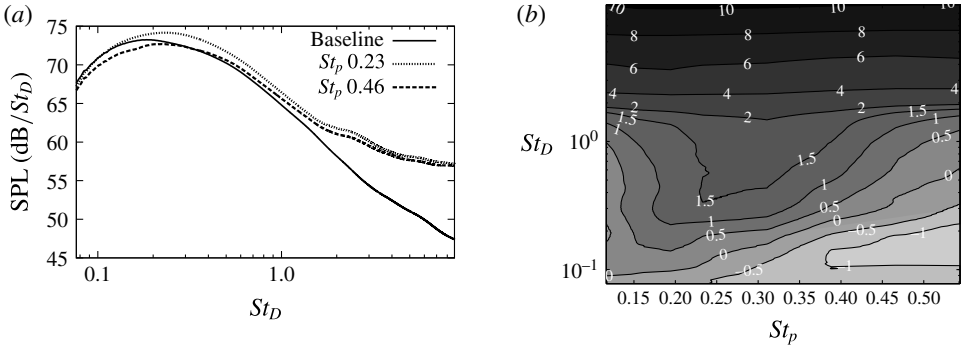


FIGURE 5. (*a*) Baseline and controlled noise spectra at 20° and Mach 0.3, $U_{mic} =$ 240 m s^{-1}; the perturbation frequencies are St_p0.23 and St_p0.46. (*b*) Change in noise (contours in dB) as a function of the perturbation Strouhal number and Strouhal number.

of the system as a function of the perturbation frequency, the far field being measured at a single point.

The time-periodic motion of the actuator generates tonal self-noise, predominantly at St_p, but the jet is also excited at this Strouhal number, and the resulting coherent periodic motion also radiates tonal sound. One cannot easily distinguish the parts of the far-field sound corresponding to actuator self-noise and flow response at St_p. Accordingly, for clarity, and similarly to other studies of periodically forced jets (Moore 1977; Laufer & Yen 1983), a notch filter was applied in order to focus on the broadband response of the jet. The raw spectrum, prior to the filtering, is presented in figure 4, for the flow controlled at $St_p = 0.46$.

Once the acoustic spectra are smoothed by the notch filter, it is possible to evaluate more clearly the impact of actuation on the broadband sound. The result, summarised in figure 5, has three features of note. A high-frequency noise increase is observed at $St_D > 2$, where $St_D = fD/U_{jet}$ is the Strouhal number corresponding to a given frequency f and U_{jet} is the jet velocity. We associate this with scattering, by the plug, of turbulence associated with the interaction between the main- and control-jet flows: we have established that this component of the noise has a lower velocity scaling than the jet noise, and is no longer measurable at higher Mach numbers. This is shown in figure 6, where sound pressure spectra are shown with and without a velocity

https://doi.org/10.1017/jfm.2015.670 Published online by Cambridge University Press

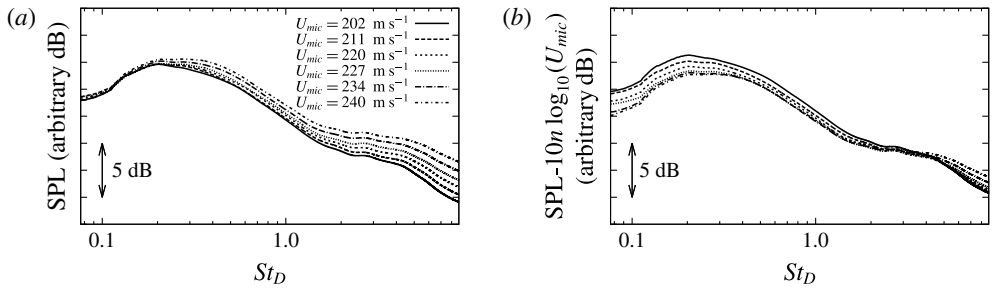


FIGURE 6. Noise spectra at 30° and Mach 0.3 controlled at $St_p0.30$ with different microjet exit velocities (*a*) without velocity scaling and (*b*) with velocity scaling (n exponent approximately 3).

scaling ($U^3_{microjet}$) based on the control-jet velocity. Other than jet interaction noise, a high-frequency penalty is expected due to the incoherent turbulence generated in the jet (Bridges & Brown 2004). Although it is currently impossible to separate the two contributions, as the speed of the microjets is increased, the former is expected to influence the total acoustic sound radiation less.

The second feature of interest is the monotonic increase, with perturbation frequency, of the crossover frequency between noise reduction and noise increase. Future studies, using a new, more rapid, prototype will establish whether this trend continues.

The third feature is the difference between the response of the jet to low- and high-frequency actuation. For low rotation speeds the acoustic radiation is increased, whereas when the rotation speed is increased there is a reduction of low-frequency sound. This is exemplified in figure 5 for two rotation Strouhal numbers. For $St_p = 0.23$ there is a sound increase for all frequencies, and in what follows this flow will be labelled as the louder jet. On the contrary, for $St_p = 0.46$ there is noise reduction for Strouhal numbers close to the peak radiation; accordingly, we label this as the quieter jet. In the following sections we study these two flows in some detail to get a sense of the mechanisms that lead to an increase or a reduction of the sound radiation.

3.2. *In the aerodynamic field*

Some global indicators of the flow response to actuation are shown in figures 7 and 8. The mean-field deformation in the near-nozzle region is similar at both rotation frequencies, except on the centreline, where an increase in mean velocity is observed with increasing actuation frequency, indicating, incidentally, that a drag reduction may also result. Farther downstream, the low-frequency actuation leads to a significant reduction in mean centreline velocity; at the higher frequency a smaller reduction is observed. As the frequency is increased, the flow is thus seen to respond differently in the upstream and downstream regions. Figure 7(*a*) shows that in the near-plug region, as the actuation frequency is increased, the flow is progressively accelerated on the centreline; in the downstream region ($x/D > 5$), on the other hand, the flow undergoes a substantial deceleration in response to low-frequency actuation, a subsequent acceleration being observed as the actuation frequency is increased. We note, nonetheless, that the two controlled profiles have similar shapes: both entrain and redistribute axial momentum towards the centreline in the initial

https://doi.org/10.1017/jfm.2015.670 Published online by Cambridge University Press

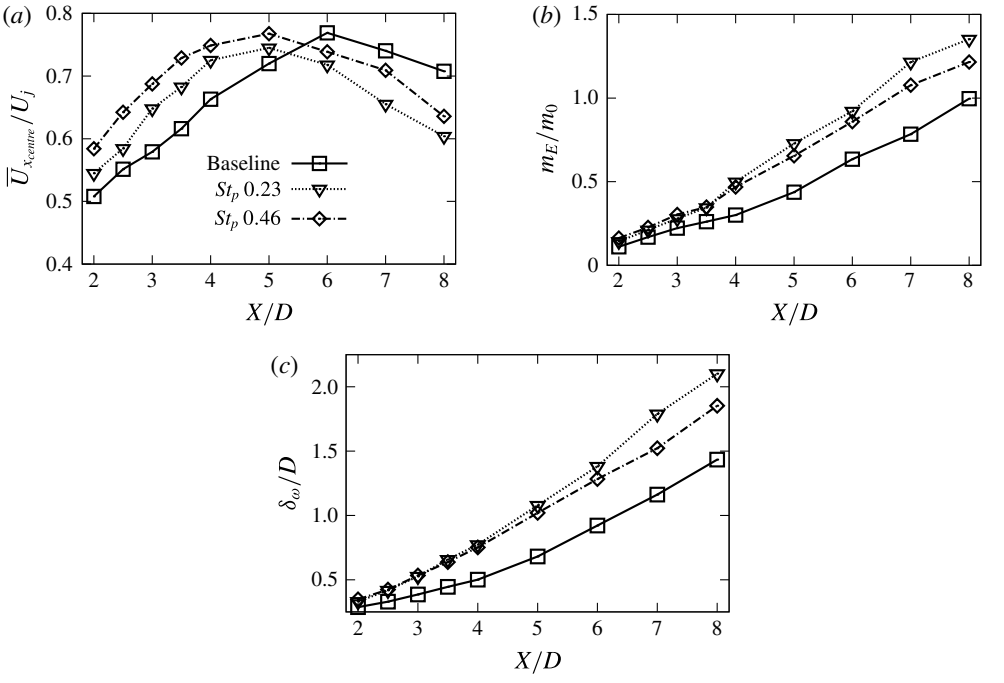


FIGURE 7. Longitudinal evolution of (*a*) the mean axial velocity on the jet centreline, (*b*) the vorticity thickness and (*c*) the entrainment of the baseline and controlled jets at $St_p0.23$ and $St_p0.46$.

region. Such redistribution of axial momentum, with the flow being slowed down for positions close to the centreline, is also seen for large r/d, as shown in figure 8. Both controlled flows have lower shear than the baseline jet. This is significant for the linear stability of the flow, as a reduction of the shear can be expected to favourably modify the dynamics of instability waves. This will be explored further in the next section.

The entrainment, shown in figure 7(*b*), is impacted in a similar manner at the two actuation frequencies up to $x/D = 4$, indicating that the higher centreline velocity observed in this region at the $St_p = 0.46$ test point is due to redistribution rather than additional entrainment. Downstream of $x/D = 4$, it is the lower-frequency actuation that produces greater entrainment; we again note the non-monotonic character of this behaviour. Similar conclusions on the non-monotonic behaviour can be drawn by observing the vorticity thickness in figure 7(*c*).

The turbulent kinetic energy, presented in figure 9, is similarly enhanced at both frequencies in the near-nozzle region, whereas downstream of $x/D = 3$, after a large increase at $St_D = 0.23$, it decreases at $St_D = 0.46$ to the point where the peak levels drop below that of the baseline downstream of $x/D = 6$. The normal components of the Reynolds stress tensor (not shown) show a similar behaviour, indicating that the energisation is more or less isotropic.

In what follows, an analysis of the (ω, m) structure of the near-plug velocity field will help us to understand the very different axial evolutions of the fluctuation energy in the two cases: both flows are excited with the same amplitude, but with quite different spatiotemporal characteristics, provoking, as a consequence, quite different responses in the downstream region.

https://doi.org/10.1017/jfm.2015.670 Published online by Cambridge University Press

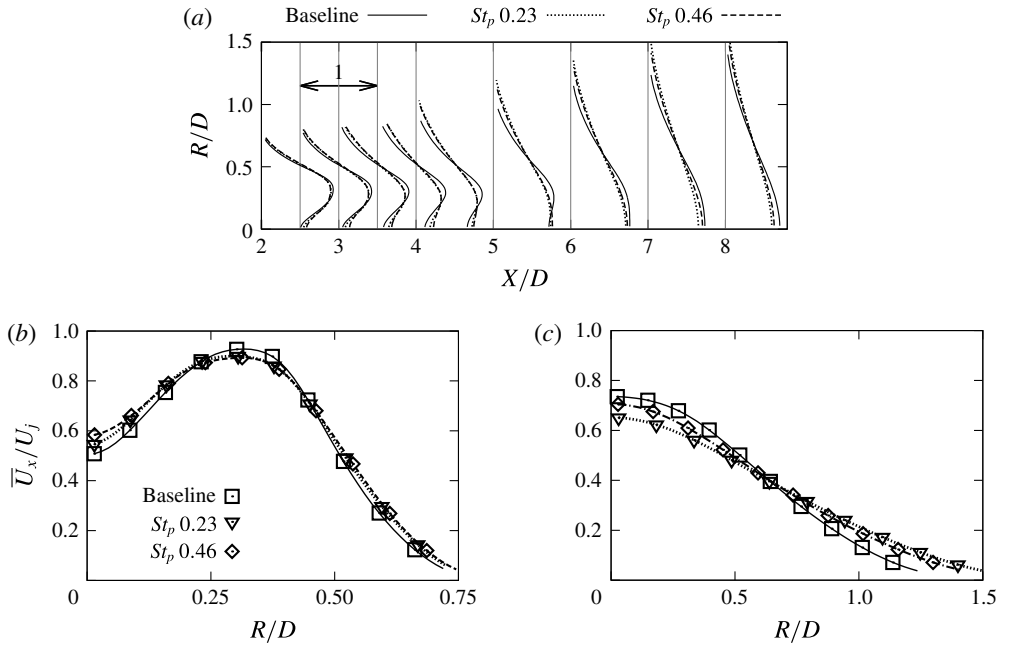


FIGURE 8. (*a*) Mean axial velocity $\overline{U}_x/U_j$; (*b*) zoom on radial profile at $x/D = 2$; (*c*) zoom on radial profile at $x/D = 7$.

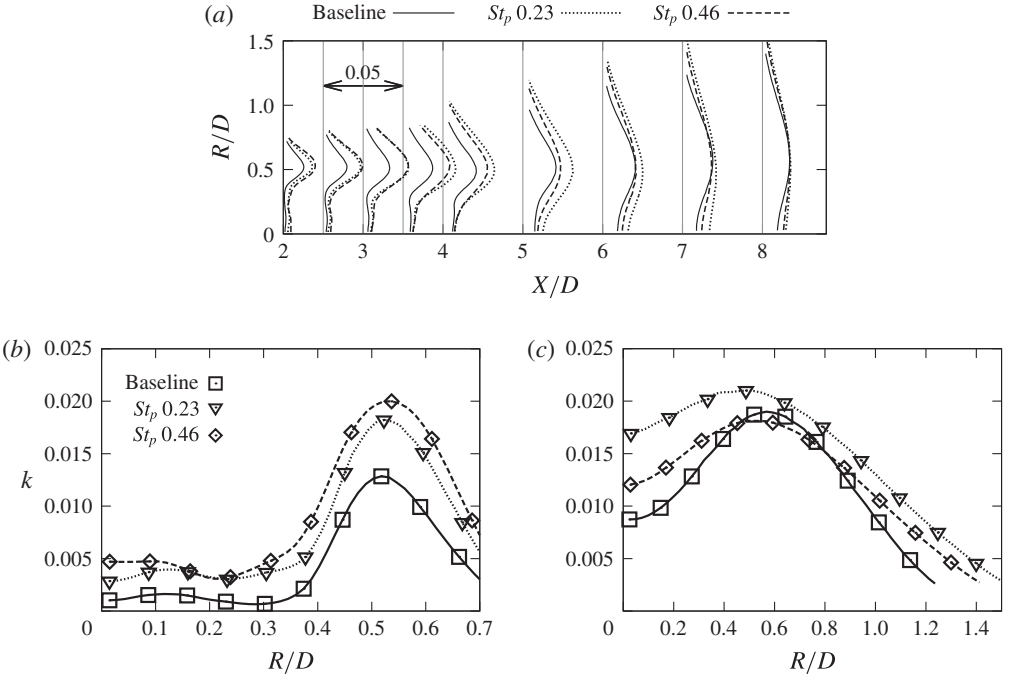


FIGURE 9. (*a*) Turbulent kinetic energy profile; (*b*,*c*) zoom on radial profiles of turbulent kinetic energy for (*b*) $X = 2D$ and (*c*) $X = 7D$.

https://doi.org/10.1017/jfm.2015.670 Published online by Cambridge University Press

4. Analysis and interpretation

As discussed earlier, the modelling of wavepackets involves a linearisation of the Navier–Stokes system about the turbulent mean. Explicit nonlinear interactions between wavepackets are thus neglected. Nonlinearity is, however, implicitly present in the base flow, as this is established by Reynolds stresses associated with the nonlinearly interacting energy-containing eddies. Manipulation of these eddies can provoke a change in the Reynolds stresses, with which there will be an associated change in the mean flow, and, consequently, the dynamics of linear waves.

The following wavepacket characteristics are known to be important where their acoustic efficiency is concerned: (1) their fluctuation amplitudes, (2) the shape of their amplitude envelopes, (3) their phase velocities and (4) their 'jitter' (Cavalieri *et al.* 2011*b*; Jordan & Colonius 2013). The fluctuation amplitude cannot be directly obtained from a linear model, which involves a free constant that can only be determined by matching with experimental data; nor can wavepacket 'jitter' be usefully quantified by current linear models: this challenging issue is the object of ongoing research by this and other groups (Zhang *et al.* 2014, 2015). On the other hand, information pertaining to the amplitude envelopes and phase speeds can be provided by linear theory. Locally parallel theory provides a first approximation of the growth rate at a given axial position, while PSE can be used to compute its axial evolution, taking into account the slowly varying change of the mean flow. Phase speeds can also be obtained, and we note that the dependence of sound radiation on this wavepacket parameter is exponential (Crow 1972; Cavalieri *et al.* 2011*b*).

We hypothesise that the quieter flow results from a modification of the mean flow, with which there is an associated change in acoustically relevant wavepacket dynamics, and we use linear theory to provide what information it can in this regard. A final caveat regarding linear theory is necessary before we proceed. A substantial body of work has been dedicated to its comparison with data issued from both experiment and computation. Until recently, these comparisons have shown compelling agreement in the Strouhal number range $0.3 < St \leqslant 1$; a more recent unpublished study by three of the present authors (Sasaki, Cavalieri & Jordan) has shown that this range can be extended to $0.3 < St \leqslant 2$. Linear theory does not show such good agreement at the lowest frequencies however, and this is a subject of ongoing study. The sound reductions we observe are in the range $St < 0.3$, i.e. in precisely that range where we cannot entirely trust growth-rate predictions. Only limited growth-rate results will therefore be presented in what follows, and these should be treated with caution, bearing in mind what we have said here. Phase velocities, on the other hand, are predicted with good accuracy over the entire spectrum of relevant frequencies (Gudmundsson & Colonius 2011; Breakey *et al.* 2013). More solid conclusions that can thus be drawn when considering this wavepacket parameter, on which, as mentioned above, the sound field exhibits exponential dependence.

As discussed in the introduction, the rotating microjets lead to time-periodic fluctuations at the microjet-passing frequency, but also to broadband disturbances related to turbulence generated by the interaction between the control jets and the main jet. *A priori* both may lead to Reynolds stresses that affect the mean field, and hence the wavepacket dynamics.

A triple decomposition of the flow variables (Hussain & Reynolds 1970) is useful in this context. For the axial velocity component, for instance, we have

$$u = \overline{U} + \tilde{u} + u', \tag{4.1}$$

where the axial velocity u is written in terms of its mean value, $\overline{U}$, a time-periodic component, $\tilde{u}$, related to the rotating actuator, and a fluctuation, u', that comprises both incoherent turbulence and non-periodic wavepacket motion.

https://doi.org/10.1017/jfm.2015.670 Published online by Cambridge University Press

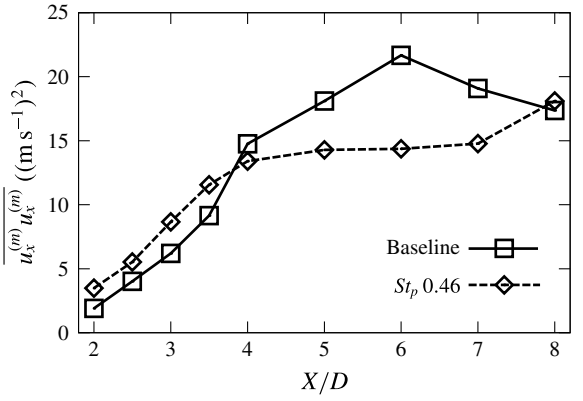


FIGURE 10. Axial evolution of the fluctuating energy of the axisymmetric component of the axial velocity.

4.1. *The quieter flow: stabilisation of axisymmetric wavepackets*

We first consider the quieter $St_p = 0.46$ case, and note that the greatest noise reduction is observed at low emission angles, where the sound field is known to be predominantly axisymmetric (Juvé, Sunyach & Comte-Bellot 1979; Kopiev *et al.* 2010; Cavalieri *et al.* 2012*a*) and dominated by a source mechanism driven by the axisymmetric component of the axial velocity fluctuation (Michalke & Fuchs 1975; Cavalieri *et al.* 2013). This sound source is considered by many (Jordan & Colonius 2013) to comprise an axially extended non-compact wavepacket, understood as an instability of the mean field. We therefore examine the axial evolution of the fluctuation energy of the axisymmetric component of the velocity field, provided by a Fourier-series decomposition of the TR-PIV data and shown in figure 10. Reductions of up to 25 % are observed for the quieter flow downstream of $x/D = 4$.

This reduction can be understood as due to a change in the dynamics of linear instabilities on account of a mean-field deformation produced by the actuation, which alters the growth rates and phase velocities of the fluctuations. A linear stability analysis using the measured mean velocity profiles is used to explore this assertion. We solve the linear PSE using the experimental mean flows from $x/D = 2$ to 5 (sufficiently discretised mean-flow data were not available farther downstream). Details of the calculation and validation are given in the appendix A.

Let us first consider the growth-rate predictions. As the PSE includes the effect of mean-flow divergence, the growth rates are a function of radius and differ depending on the flow variable considered (Crighton & Gaster 1976) (for further comments on the PSE, the reader is referred to the appendix A). We therefore consider the local wavenumber $\alpha(x)$ from the PSE ansatz,

$$\boldsymbol{q}(\boldsymbol{x}, t) = \hat{\boldsymbol{q}}(x, r)\, \mathrm{e}^{\mathrm{i} \int \alpha(x)\, \mathrm{d}x}\, \mathrm{e}^{\mathrm{i}m\theta}\, \mathrm{e}^{-\mathrm{i}\omega t}, \tag{4.2}$$

which is responsible for the fast (i.e. exponential) axial evolution of disturbances within the jet. Accordingly, the imaginary part of α provides an average amplification throughout the flow and for all fluctuations. The changes for different flow quantities and radial positions are absorbed in the slowly changing function $\hat{\boldsymbol{q}}$, and are less significant in comparison to the exponential growth in the integral of equation (4.2).

https://doi.org/10.1017/jfm.2015.670 Published online by Cambridge University Press

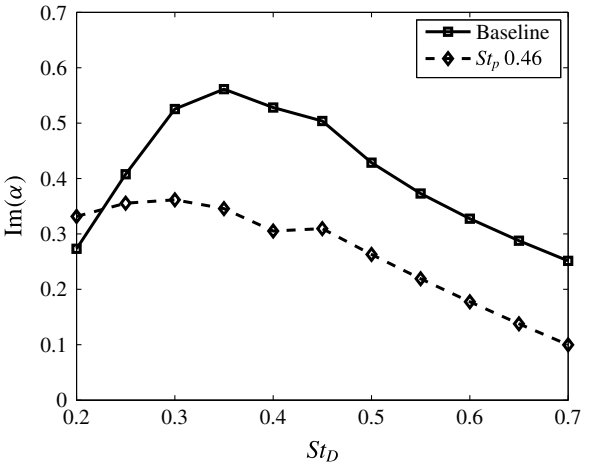


FIGURE 11. Growth rates of the azimuthal mode $m = 0$ at $X = 4D$, as a function of frequency, for baseline and $St_p = 0.46$ actuation.

Figure 11 shows the PSE predictions for growth rates at $X = 4D$ (i.e. towards the end of the region over which PSE computations were possible) in the baseline and 'quiet' flow. Substantial growth-rate reductions are manifested over a large frequency range, consistent with the experimental data presented in figure 10, which show suppressed fluctuation energy for azimuthal mode $m = 0$ (integrated over all frequencies) downstream of $X = 4D$. This is an indication that the actuation has led to an acoustically useful mean-flow deformation where this wavepacket parameter is concerned.

An average phase velocity, $U_c/c = \omega/\alpha_r$ (with α_r corresponding to the real part of the wavenumber, α, and c the ambient speed of sound), can also be defined. Figure 12, which presents the PSE predictions of phase velocity for the baseline and controlled flows at four axial positions, shows that the PSE predicts lower phase velocities for the actuated flow for all positions and frequencies considered. For the three most downstream positions the phase-velocity reduction is greatest at low frequency. As discussed earlier, this wavepacket parameter is known to be predicted with good accuracy by the PSE; it is a parameter on which the radiated sound depends exponentially. It is therefore probable that this modification is the most significant where the observed sound reduction is concerned.

We have seen, using linear PSE results for the evolution of wavepackets, that the controlled jet has lower streamwise amplifications and phase velocities than the baseline case, which may explain the observed reductions in radiated sound. Since the predicted wavepackets are linearised solutions taking the mean field as the base flow, the differences must be related to changes in the mean flow. In what follows we examine the mechanisms that underpin mean-flow changes in the actuated jet.

The mean-flow deformation can be understood by considering the mean momentum balance for the axial velocity component, written in terms of a triple decomposition of the axial velocity, $u = \overline{U} + \tilde{u} + u'$,

$$\rho_0 \left(\overline{U}_x \frac{\partial \overline{U}_x}{\partial x} + \overline{U}_r \frac{\partial \overline{U}_x}{\partial r} \right) = -\frac{\partial \overline{P}}{\partial x} + \mu \overline{S}_x - \rho_0 \left(\frac{\partial (\overline{\tilde{u}_x^2} + \overline{u_x'^2})}{\partial x} + \frac{1}{r} \frac{\partial (r\overline{\tilde{u}_x \tilde{u}_r} + r\overline{u_x' u_r'})}{\partial r} \right), \tag{4.3}$$

https://doi.org/10.1017/jfm.2015.670 Published online by Cambridge University Press

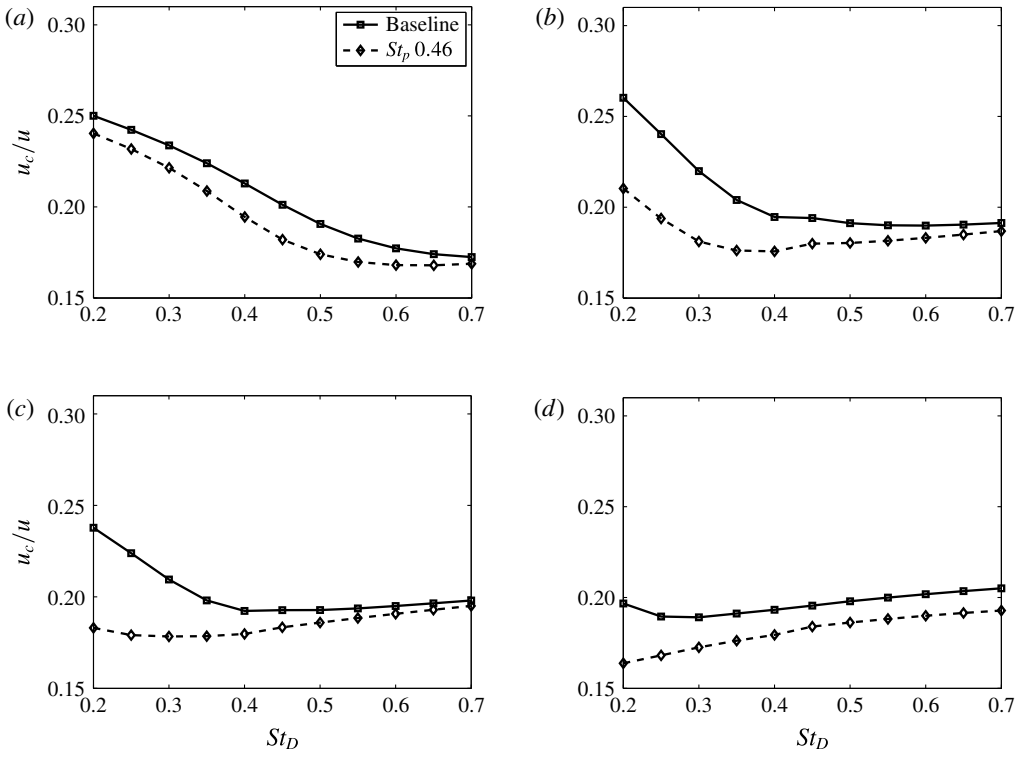


FIGURE 12. Phase speeds predicted by the PSE for the baseline and controlled flows: (*a*) $X/D = 2$, (*b*) $X/D = 3$, (*c*) $X/D = 4$, (*d*) $X/D = 5$.

where ρ_0 is the density, U_x and U_r are the mean axial and radial velocity components, P is the mean pressure field, μS_x are the viscous forces along the axial direction, u_x and u_r are the axial and radial velocity fluctuations and r is the radial distance.

Deformation of the mean field can be produced by both coherent and incoherent Reynolds stresses. The former is associated with a harmonic response of the flow to the harmonic component of the perturbations introduced by actuation, i.e. at $(St_P, m) = (0.46, 2)$, while the latter is associated with non-harmonic components (e.g. small-scale structures generated as the exit flow interacts locally with the two wall jets). If the flow is unstable to the harmonic component of the actuation structure, the response will comprise harmonic wavepackets, phase-locked to the actuation; if it is unstable to any part of the stochastic component of the perturbations produced by actuation, stochastic wavepackets (difficult to distinguish from the wavepackets driven by the boundary-layer structure) will be produced; finally, if the jet is stable to both the harmonic and stochastic components due to actuation, wavepackets will not arise, and the response to actuation will comprise incoherent turbulence.

The triple decomposition allows identification of the contributions of the harmonic and stochastic components of the flow response to the Reynolds stresses that underpin the mean-flow structure. Figure 13, which shows the difference between the baseline and controlled-flow Reynolds stresses contributing to the streamwise momentum balance, indicates that the mean-flow deformation is dominated by the stochastic component of the Reynolds stresses. This demonstrates that the response of the flow to actuation is dominated by stochastic flow motions. That this is turbulence

https://doi.org/10.1017/jfm.2015.670 Published online by Cambridge University Press

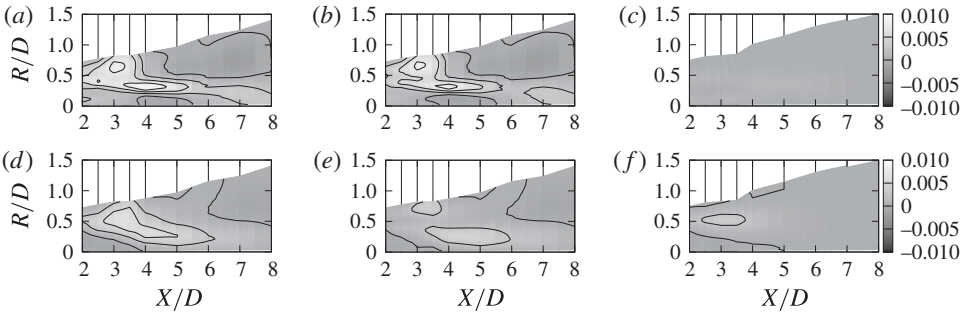


FIGURE 13. Contribution of the non-cyclic and cyclic components in the Reynolds stress tensor comparatively to the baseline jet for $\overline{u_x' u_x'}$ (*a–c*) and $\overline{u_x' u_r'}$ (*d–f*): (*a*,*d*) total; (*b*,*e*) non-cyclic part; (*c*,*f*) cyclic part.

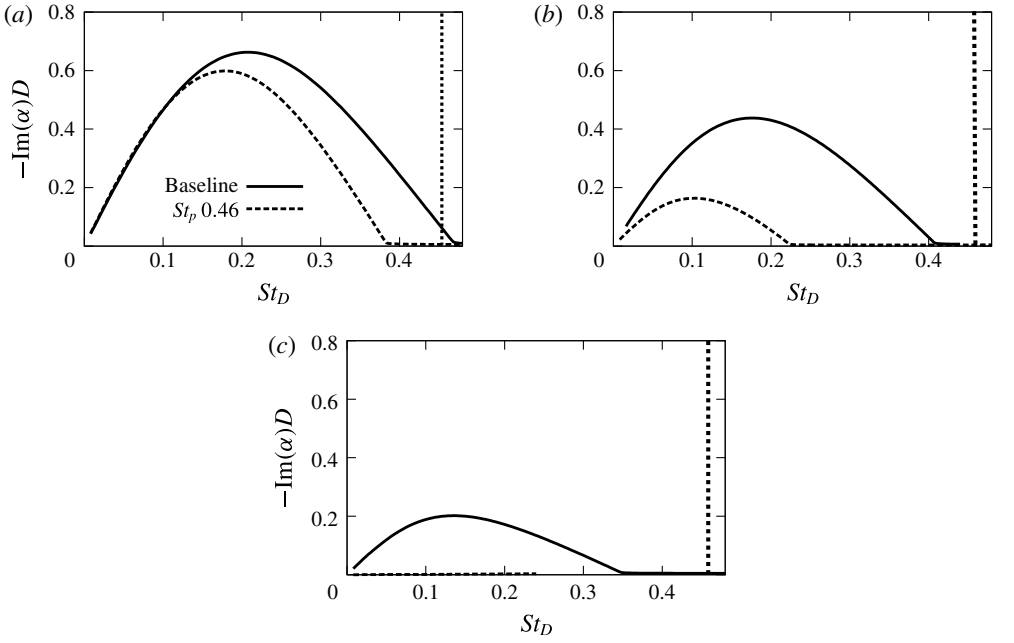


FIGURE 14. Growth rates of the azimuthal mode $m = 2$, as a function of frequency, for baseline and $St_p = 0.46$ actuation: (*a*) $X = 2D$, (*b*) $X = 2.5D$, (*c*) $X = 3D$.

rather than stochastic wavepackets is suggested by an estimate of the characteristic frequencies associated with the local interaction between the exit flow and the two wall jets: vortex shedding from the wall jets (of diameter $d = 0.0013$) will occur at $St_D \approx 6.15$; it is clear that the jet is stable to such a perturbation. This supports the contention that the response of the flow to the high-frequency actuation predominantly comprises turbulence rather than coherent structures.

We now postulate that the dynamics of the flow response to actuation primarily comprises incoherent turbulence because the actuation energises the flow with an (ω, m) structure to which the mean field is stable. A linear stability analysis shows (cf. figure 14) that the mean field is indeed everywhere stable to the actuation

https://doi.org/10.1017/jfm.2015.670 Published online by Cambridge University Press

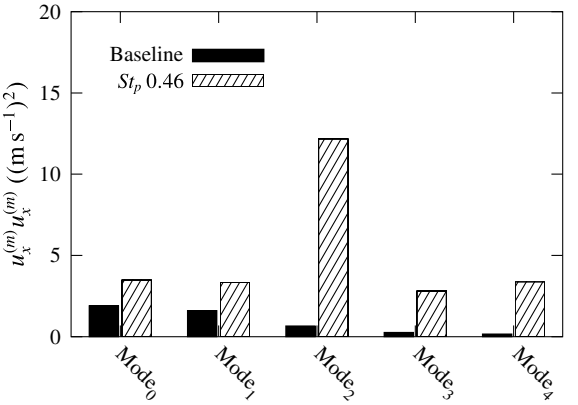


FIGURE 15. Fluctuation energy of azimuthal modes of the axial velocity component in the near-plug region ($x/D = 2$) at $R = 0.25D$ (where peak levels are observed).

structure ($St_p = 0.46$, $m = 2$), and so we conclude that the considerable fluctuation energy introduced into the system by the actuation at azimuthal mode $m = 2$ evolves downstream as incoherent turbulence, producing a mean-field deformation on which axisymmetric linear waves, which dominate downstream radiation, have lower growth rates and phase speeds than in the baseline flow. Figure 15 shows the considerable fluctuation energy introduced in the field at the $m = 2$ mode; similar trends are seen in areas within the near-plug region of the jet (Kœnig 2011).

With this we have a phenomenological interpretation linking the actuation to the far field. We note that the results of a number of other jet-noise control studies are consistent with this: noise abatement is most efficient when flows are driven with high ω–m combinations (Samimy *et al.* 2007; Kopiev *et al.* 2010). While we cannot affirm that the mean fields are in those cases stable to such actuation, this does seem likely, as the canonical mean field of a round subsonic jet is most stable to high frequencies and high azimuthal wavenumbers.

In the next section we consider the louder flow in a similar framework, but find that the behaviour is in this case fundamentally different.

4.2. *The louder flow: nonlinear wavepacket dynamics*

As an explanation for the different response of the flow to the actuation at $St_p = 0.23$, we postulate that this low-frequency actuation introduces high levels of fluctuation energy with an ω–m structure to which the mean field is unstable. This fact is confirmed in figure 16, which shows the results of a linear stability analysis, for the azimuthal mode $m = 2$, of both the baseline and actuated mean fields. In both cases, the actuation frequency lies close to the most unstable frequency of the mean field.

Consequently, coherent excitation at this ω–m unstable pair would lead to exponential growth of disturbances at the excitation frequency, which would then lead to nonlinear interactions. The results suggest, furthermore, that when nonlinear wavepacket interactions are present in a subsonic jet, the radiated noise levels are increased above those of the canonical unforced flow.

Figure 17 compares the fluctuation energy of the azimuthal mode $m = 0$ between the baseline and louder flows. In this case we see a slight global increase of the latter. Application of the triple decomposition here shows, contrary to the $St_p = 0.46$ case,

https://doi.org/10.1017/jfm.2015.670 Published online by Cambridge University Press

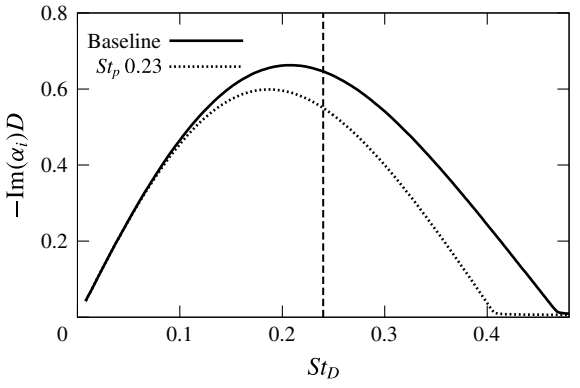


FIGURE 16. Growth rates, at $x/D = 2$, as a function of frequency for the azimuthal mode $m = 2$, for baseline and $St_p = 0.23$ actuation.

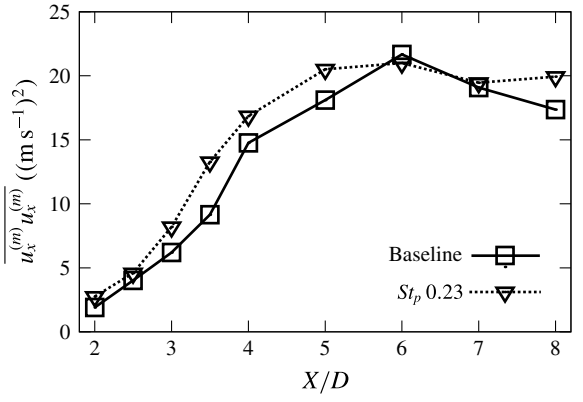


FIGURE 17. Axial evolution of the fluctuating energy of azimuthal mode 0 for the axial velocity component.

that most of the fluctuation energy is contained in the cyclic component. Figure 18, which shows six frames of the phase-averaged field over one complete period, reveals a pattern that repeats twice during that period: a frequency doubling appears to occur, indicating a quadratic wave interaction between the fundamental frequency and itself.

This is confirmed by analysis of hot-wire data. Figure 19(*a*) shows velocity power spectra of the baseline and controlled flows. These were measured at the centre of the mixing layer at $x/D = 1.5$. In the $St_p = 0.46$ case a large spike is seen at the actuation frequency, but there are no harmonics. In the $St_p = 0.23$ case, on the other hand, we see a large spike at the fundamental frequency, and this is accompanied by a series of harmonics. A bicoherence analysis shows (cf. figure 19) levels of over 40 % at $(St_D, St_D) = (0.23, 0.23)$, confirming that the first of these harmonics results from a nonlinear interaction of the fundamental with itself. The response of the flow to actuation at the lower frequency is thus seen to comprise nonlinear wavepacket dynamics, which are known to be considerably more efficient in the generation of low-angle sound (Suponitsky, Sandham & Morfey 2010).

https://doi.org/10.1017/jfm.2015.670 Published online by Cambridge University Press

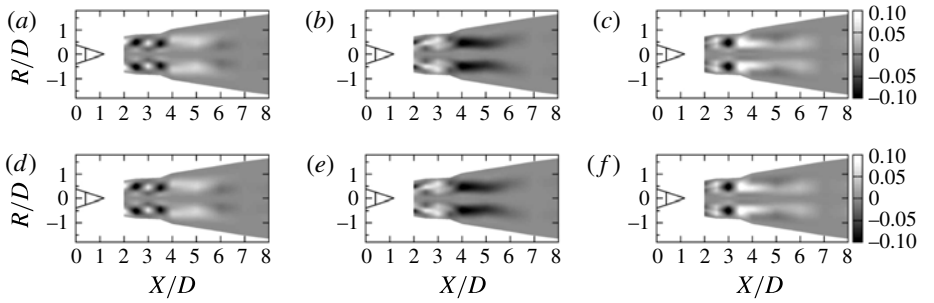


FIGURE 18. Phase-averaged field of the axial cyclic component for the $St_p = 0.23$ case. The phase is varying from $-\pi$ to $2\pi/3$ in steps of $\pi/3$: (*a*) $-\pi$, (*b*) $-2\pi/3$, (*c*) $-\pi/3$, (*d*) 0, (*e*) $\pi/3$, (*f*) $2\pi/3$.

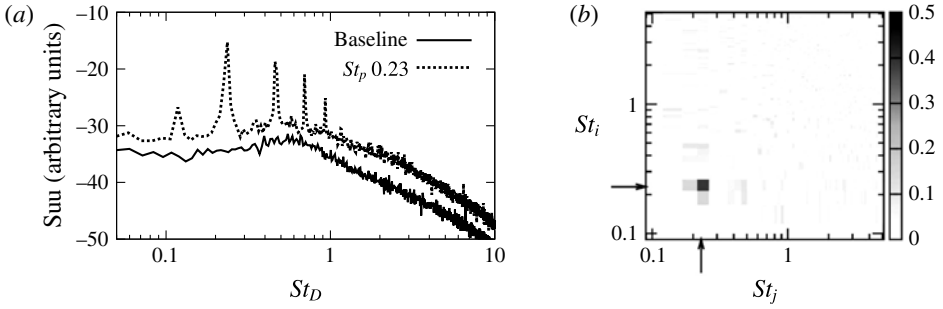


FIGURE 19. (*a*) Hot-wire spectra in the mixing layer at $X = 1.5D$ for the baseline jet and the controlled jets at $St_p0.23$; (*b*) bicoherence in the mixing layer at $X = 1.5D$, showing nonlinear interaction of $St_p0.23$ with itself.

5. Conclusions

An experimental investigation of subsonic jets subjected to perturbations introduced by means of fluidic injection from a spinning centrebody has been performed. Fluctuation energy is introduced to the flow at the azimuthal mode $m = 2$ (extension of this work to values $m > 2$ is an ongoing project by this group, and preliminary results indicate similar trends) and over the perturbation Strouhal number range $0 < St_p < 0.5$. At low frequency the acoustic response of the flow comprises a noise increase, while at higher frequencies peak noise levels are reduced. The louder and quieter flows are analysed and the mechanisms at work are shown to be quite different.

The control mechanism in the case of the high-frequency actuation involves the generation of incoherent turbulence and an associated change in the mean field. The latter comprises a reduction of mean velocity gradients, and this leads to a reduction of the growth rates and phase velocities of axisymmetric wavepackets – understood as linear instabilities of the mean flow and which are known to dominate low-angle emission. The mean-field deformation is shown, by a triple decomposition, to result from the energisation of incoherent turbulence, which arises because the high-frequency actuation introduces fluctuation energy with an ω–m structure to which the mean field is stable.

The louder flow has velocity gradients similar to the high-frequency case, and therefore instability amplification rates and phase velocities of similar order. However,

https://doi.org/10.1017/jfm.2015.670 Published online by Cambridge University Press

the actuation in this case is at frequencies to which the mean flow is unstable. Forcing in this manner leads to instability waves with initial amplitudes that are considerably greater than those of the unactuated flow, and which have a deterministic phase. Organised instability waves thus grow to a point where their amplitudes are large enough for significant nonlinear interactions to take place and dominate the flow dynamics: both the peaks and the broadband fluctuation levels are considerably enhanced and a louder jet results.

This study provides a demonstration of two very different kinds of control, and provides guidance for noise-control strategies. Actuators capable of producing mean-field deformations that lead to reduced shear have a good chance of producing a beneficial effect in terms of noise reduction by reducing the amplification rates and phase velocities of wavepackets – a mean-field effect. In the present work this deformation was shown to be due to the production of incoherent turbulent Reynolds stresses by forcing at stable ω–m combinations. However, there are certainly other means by which such a mean-field deformation might be produced (simple changes in the nozzle geometry for instance). The control mechanism demonstrated in the case of the louder jet may also be of interest where noise control is concerned: forcing a jet at unstable ω–m combinations can produce strong deterministic dynamics. While producing a louder jet in the present study, this kind of forcing is what is necessary for closed-loop control strategies, and, accompanied by a reduced-order model for the wavepacket dynamics (such as linear PSE), may allow for the real-time manipulation of the acoustic efficiency of sound-source dynamics, for the problem of jittering wavepackets for instance (Cavalieri *et al.* 2011*b*; Zhang *et al.* 2012).

Appendix A

The parabolised stability equations (PSE) apply to flows with mild streamwise variations, which allow for an extension of the parallel flow linear stability problem. In this case, the fluctuation term on the triple decomposition (4.1) is decomposed into a time-averaged axisymmetric component $\overline{\boldsymbol{q}}(\boldsymbol{x})$ and a time-dependent fluctuation $\boldsymbol{q}'(\boldsymbol{x}, t)$, where $\boldsymbol{q} = [u_x, u_r, u_\theta, \rho, T]^{\mathrm{T}}$ represents the flow variables (axial, radial and azimuthal components of velocity, density and temperature respectively) and cylindrical coordinates $\boldsymbol{x} = [x, r, \theta]$ are considered.

Given that the mean flow is homogeneous along the azimuthal and time directions, the fluctuation could be expressed in terms of normal modes in these directions,

$$\boldsymbol{q}'(\boldsymbol{x}, t) = \sum_{\omega} \sum_{m} \tilde{\boldsymbol{q}}(x, r)\, \mathrm{e}^{\mathrm{i}m\theta}\, \mathrm{e}^{-\mathrm{i}\omega t}, \tag{A 1}$$

with $\tilde{\boldsymbol{q}}$ representing the complex amplitude for a given frequency ω and azimuthal wavenumber m.

The solution may be further simplified by considering the wavepacket ansatz for slowly diverging jets (Crighton & Gaster 1976): $\tilde{\boldsymbol{q}}(x, r)$ is decomposed into two separate contributions, a slowly varying function $\hat{\boldsymbol{q}}$ and a fast oscillatory function which captures the wave-like axial structure and the exponential amplification,

$$\boldsymbol{q}'(\boldsymbol{x}, t) = \hat{\boldsymbol{q}}(x, r)\, \mathrm{e}^{\mathrm{i}\int^x \alpha(x')\,\mathrm{d}x'}\, \mathrm{e}^{\mathrm{i}m\theta}\, \mathrm{e}^{-\mathrm{i}\omega t}, \tag{A 2}$$

where $\alpha = \alpha_r + \mathrm{i}\alpha_i$ is the complex axial wavenumber, whose imaginary part will define growth or decay of disturbances along the axial direction.

https://doi.org/10.1017/jfm.2015.670 Published online by Cambridge University Press

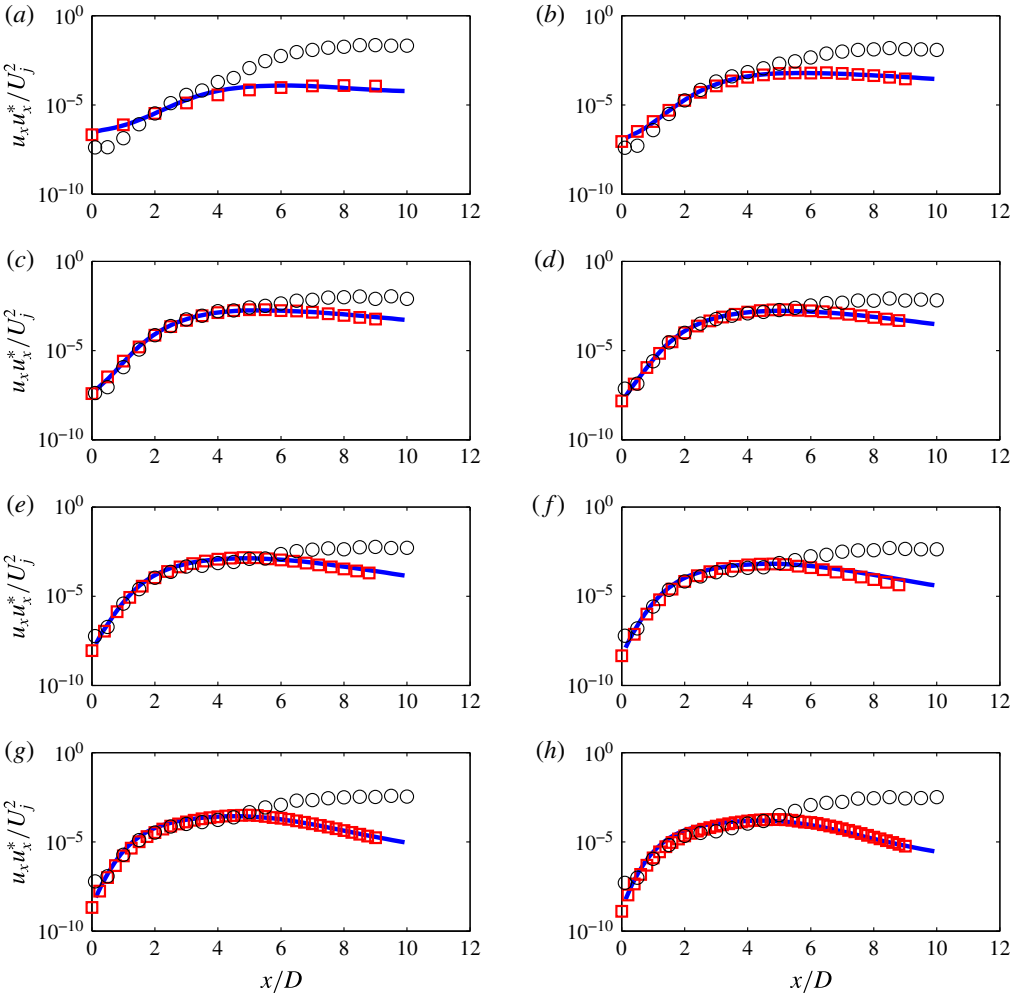


FIGURE 20. (Colour online) Centreline power spectral densities of the axial velocity – comparison between the implemented PSE method (squares) and data presented in Cavalieri *et al.* (2013): earlier PSE calculation (solid line) and experimental values obtained from hot-wire measurements (circles), for (*a*) $St = 0.2$, (*b*) $St = 0.3$, (*c*) $St = 0.4$, (*d*) $St = 0.5$, (*e*) $St = 0.6$, (*f*) $St = 0.7$, (*g*) $St = 0.8$, (*h*) $St = 0.9$.

By replacing the wavepacket ansatz (A 2) in the linearised, compressible Euler, energy and continuity equations, a matrix system is obtained,

$$(A(\overline{\boldsymbol{q}}) + B(\overline{\boldsymbol{q}}, \alpha, \omega))\hat{\boldsymbol{q}} + C(\overline{\boldsymbol{q}})\frac{\partial \hat{\boldsymbol{q}}}{\partial x} + D(\overline{\boldsymbol{q}})\frac{\partial \hat{\boldsymbol{q}}}{\partial r} = 0, \tag{A 3}$$

where the high Reynolds number of the flows considered justifies the neglect of the viscous terms. Linearisation allows the independent calculation of each ω–m combination.

A second condition must be added to the PSE system (A 3) in order to eliminate the ambiguity between $\hat{\boldsymbol{q}}$ and α. This is done by forcing the spatial growth to be absorbed solely by the complex amplitude $\mathrm{e}^{\mathrm{i}\int \alpha(x')\,\mathrm{d}x'}$. This is ensured by the

https://doi.org/10.1017/jfm.2015.670 Published online by Cambridge University Press

normalisation proposed in Herbert (1997),

$$\int_0^\infty \hat{\boldsymbol{q}} \frac{\partial \hat{\boldsymbol{q}}*}{\partial x} r \, \mathrm{d}r = 0. \tag{A 4}$$

A pseudospectral method is used to discretise the radial derivatives, with functions described by means of Chebyshev polynomials. The axial derivatives are calculated using finite differences, and Dirichlet boundary conditions are used to define the flow variables at $r \to \infty$.

The first step of the numerical method uses the parallel flow approximation to construct a spatial linear stability problem, whose solution gives the initial value to start the PSE iteration. Since these are solutions to linear PSE, they are determined up to a free constant, which is chosen so as to adjust overall amplitudes to experimental data.

Finally, the experimental data for the mean flow were fitted with a Gaussian profile in order to avoid non-smoothness of the experimentally obtained data.

Further comments on the PSE theoretical background and numerical approach that was chosen may be found in Herbert (1997), Gudmundsson & Colonius (2011), Rodríguez *et al.* (2015) and Sasaki (2014).

We now briefly present a validation of the numerical method used for solution of the PSE. Figure 20 presents the axial evolution of the fluctuation energy of the axisymmetric mode of the axial velocity for a turbulent jet of Mach 0.4 and Reynolds number 4.2×10^5. Results obtained using the present code are compared with the experimental and numerical data of Cavalieri *et al.* (2013).

The PSE code used in this work closely reproduces the results of the calculation presented in Cavalieri *et al.* (2013), thus validating the present method.

For the lowest frequencies, the PSE underestimate the growth of the fluctuations, which, while a known result (Gudmundsson & Colonius 2011; Cavalieri *et al.* 2013; Sasaki 2014), has not been clearly explained in the literature. For Strouhal numbers above 0.3, the PSE reproduce the behaviour of the velocity fluctuation correctly until the end of the potential core. After $X/D = 5$, the PSE no longer reproduce the experimental data, presenting an earlier saturation, indicating that linear wavepackets may no longer dominate the dynamics of the turbulent flow in this region.

REFERENCES

BREAKEY, D. E. S., JORDAN, P., CAVALIERI, A. V. G., LÉON, O., ZHANG, M., LEHNASCH, G., COLONIUS, T. & RODRIGUEZ, D. 2013 Near-field wavepackets and the far-field sound of a subsonic jet. In *19th AIAA/CEAS Aeroacoustics Conference, AIAA Paper*, 2013-2083.

BRIDGES, J. & BROWN, C. A. 2004 Parametric testing of chevrons on single flow hot jets. *AIAA Paper* 2004–2824.

BRIDGES, J. E. & HUSSAIN, A. K. M. F. 1987 Roles of initial condition and vortex pairing in jet noise. *J. Sound Vib.* **117** (2), 289–311.

BUTLER, G. W. & CALKINS, F. T. 2003 Initial attempts to suppress jet noise using piezoelectric actuators. *AIAA Paper* 2003-3192.

CAVALIERI, A. V. G., DAVILLER, G., COMTE, P., JORDAN, P., TADMOR, G. & GERVAIS, Y. 2011*a* Using large eddy simulation to explore sound-source mechanisms in jets. *J. Sound Vib.* **330** (17), 4098–4113.

CAVALIERI, A. V. G., JORDAN, P., AGARWAL, A. & GERVAIS, Y. 2011*b* Jittering wave-packet models for subsonic jet noise. *J. Sound Vib.* **330** (18), 4474–4492.

https://doi.org/10.1017/jfm.2015.670 Published online by Cambridge University Press

CAVALIERI, A. V. G., JORDAN, P., COLONIUS, T. & GERVAIS, Y. 2012*a* Axisymmetric superdirectivity in subsonic jets. *J. Fluid Mech.* **704**, 388–420.

CAVALIERI, A. V. G., RODRIGUEZ, D., JORDAN, P., COLONIUS, T. & GERVAIS, Y. 2012*b* Wavepackets in the velocity field of turbulent jets. In *18th AIAA/CEAS Aeroacoustics Conference and Exhibit, Colorado Springs, CO, USA*.

CAVALIERI, A. V. G., RODRÍGUEZ, D., JORDAN, P., COLONIUS, T. & GERVAIS, Y. 2013 Wavepackets in the velocity field of turbulent jets. *J. Fluid Mech.* **730**, 559–592.

CRIGHTON, D. G. 1975 Basic principles of aerodynamic noise generation. *Prog. Aerosp. Sci.* **16**, 31–96.

CRIGHTON, D. G. & GASTER, M. 1976 Stability of slowly diverging jet flow. *J. Fluid Mech.* **77** (2), 387–413.

CRIGHTON, D. G. & HUERRE, P. 1990 Shear layer pressure fluctuations and superdirective acoustic sources. *J. Fluid Mech.* **220**, 355–368.

CROW, S. C. 1972 Acoustic gain of a turbulent jet. In *Phys. Soc. Meeting, Univ. Colorado, Boulder, Paper IE*, vol. 6.

CROW, S. C. & CHAMPAGNE, F. H. 1971 Orderly structure in jet turbulence. *J. Fluid Mech.* **48**, 547–591.

FFOWCS-WILLIAMS, J. E. & KEMPTON, A. J. 1978 The noise from the large-scale structure of a jet. *J. Fluid Mech.* **84**, 673–694.

FREUND, J. B. 2001 Noise sources in a low-Reynolds-number turbulent jet at Mach 0.9. *J. Fluid Mech.* **438**, 277–305.

GUDMUNDSSON, K. & COLONIUS, T. 2007 Spatial stability analysis of chevron jet profiles. *AIAA Paper* **3599**, 8–10.

GUDMUNDSSON, K. & COLONIUS, T. 2011 Instability wave models for the near-field fluctuations of turbulent jets. *J. Fluid Mech.* **689**, 97–128.

GUTMARK, E. J. & GRINSTEIN, F. F. 1999 Flow control with noncircular jets 1. *Annu. Rev. Fluid Mech.* **31** (1), 239–272.

HENDERSON, B. 2010 Fifty years of fluidic injection for jet noise reduction. *Intl J. Aeroacoust.* **9**, 91–122.

HERBERT, T. 1997 Parabolized stability equations. *Annu. Rev. Fluid Mech.* **29** (1), 245–283.

HUSSAIN, A. K. M. F. & REYNOLDS, W. C. 1970 The mechanics of an organized wave in turbulent shear flow. *J. Fluid Mech.* **41**, 241–258.

HUSSAIN, A. K. M. F. & ZAMAN, K. B. M. Q. 1981 The 'preferred mode' of the axisymmetric jet. *J. Fluid Mech.* **110** (1), 39–71.

JORDAN, P. & COLONIUS, T. 2013 Wave packets and turbulent jet noise. *Annu. Rev. Fluid Mech.* **45**, 173–195.

JUVÉ, D., SUNYACH, M. & COMTE-BELLOT, G. 1979 Filtered azimuthal correlations in the acoustic far field of a subsonic jet. *AIAA J.* **17** (1), 112–113.

KERHERVÉ, F., JORDAN, P., CAVALIERI, A. V. G., DELVILLE, J., BOGEY, C. & JUVÉ, D. 2012 Educing the source mechanism associated with downstream radiation in subsonic jets. *J. Fluid Mech.* **710**, 606–640.

KIM, K., KASNAKOLU, C., SERRANI, A. & SAMIMY, M. 2009 Extremum-seeking control of subsonic cavity flow. *AIAA J.* **47** (1), 195–205.

KŒNIG, M. 2011 Réduction de bruit de jet par injection fluidique en corps central tournant (in French). PhD thesis, ENSIP – Université de Poitiers.

KOPIEV, V., CHERNYSHEV, S., FARANOSOV, G., ZAITSEV, M. & BELYAEV, I. 2010 Correlations of jet noise azimuthal components and their role in source identification. In *16th AIAA/CEAS Aeroacoustics Conference (31st AIAA Aeroacoustics Conference)*.

LAU, J. C., FISHER, M. J. & FUCHS, H. V. 1972 The intrinsic structure of turbulent jets. *J. Sound Vib.* **22** (4), 379–406.

LAUFER, J. & YEN, T.-C. 1983 Noise generation by a low-Mach-number jet. *J. Fluid Mech.* **134**, 1–31.

https://doi.org/10.1017/jfm.2015.670 Published online by Cambridge University Press

LIU, J. T. C. 1974 Developing large-scale wavelike eddies and the near jet noise field. *J. Fluid Mech.* **62** (03), 437–464.

MANKBADI, R. & LIU, J. T. C. 1984 Sound generated aerodynamically revisited: large-scale structures in a turbulent jet as a source of sound. *Phil. Trans. R. Soc. Lond.* A **311** (1516), 183–217.

MAURY, R., KOENIG, M., CATTAFESTA, L., JORDAN, P. & DELVILLE, J. 2012 Extremum-seeking control of jet noise. *Intl J. Aeroacoust.* **11** (3), 459–474.

MAURY, R., KOENIG, M., CATTAFESTA, L., JORDAN, P., DELVILLE, J., BONNET, J. P. & GERVAIS, Y. 2009 Extremum-seeking optimisation of fluidic jet noise control. In *15th AIAA/CEAS Aeroacoustics Conference (30th AIAA Aeroacoustics Conference)*.

MICHALKE, A. 1970 *A wave model for sound generation in circular jets*. Deutsche Forschungs- und Versuchsanstalt für Luft- und Raumfa (Cologne), ID.

MICHALKE, A. 1971 Instabilitat eines kompressiblen runden Freistrahls unter Berucksichtigung des Einflusses der Strahlgrenzschichtdicke. *Z. Flugwiss. English translation: NASA TM* 75190, *1977* **19**, 311–328.

MICHALKE, A. & FUCHS, H. V. 1975 On turbulence and noise of an axisymmetric shear flow. *J. Fluid Mech.* **70**, 179–205.

MOLLO-CHRISTENSEN, E. 1963 Measurements of near field pressure of subsonic jets. *Tech. Rep.*, DTIC Document.

MOLLO-CHRISTENSEN, E. 1967 Jet noise and shear flow instability seen from an experimenter's viewpoint. *J. Appl. Mech.* **34** (1), 1–7.

MOORE, C. J. 1977 The role of shear-layer instability waves in jet exhaust noise. *J. Fluid Mech.* **80**, 321–367.

RODRÍGUEZ, D., CAVALIERI, A. V. G., COLONIUS, T. & JORDAN, P. 2015 A study of linear wavepacket models for subsonic turbulent jets using local eigenmode decomposition of PIV data. *Eur. J. Mech. (B/Fluids)* **49**, 308–321.

RODRIGUEZ, D., SINHA, A., BRES, G. A. & COLONIUS, T. 2013 Acoustic field associated with parabolized stability equation models in turbulent jets. In *19th AIAA/CEAS Aeroacoustics Conference (30th AIAA Aeroacoustics Conference), 27–29 May 2013, Berlin, Germany*.

SAMIMY, M., KIM, J.-H., KASTNER, J., ADAMOVICH, I. & UTKIN, Y. 2007 Active control of high-speed and high-Reynolds-number jets using plasma actuators. *J. Fluid Mech.* **578**, 305–330.

SANDHAM, N., MORFEY, C. & HU, Z. 2006 Sound radiation from exponentially growing and decaying waves. *J. Sound Vib.* **294**, 355–361.

SASAKI, K. 2014 Estudo e controle de pacotes de onda em jatos utilizando as equações de estabilidade parabolizadas (in Portuguese). Masters thesis, ITA – Instituto Tecnológico de Aeronáutica, São José dos Campos.

SUPONITSKY, V., SANDHAM, N. D. & MORFEY, C. L. 2010 Linear and nonlinear mechanisms of sound radiation by instability waves in subsonic jets. *J. Fluid Mech.* **658**, 509–538.

TAM, C. K. W. & MORRIS, P. J. 1980 The radiation of sound by the instability waves of a compressible plane turbulent shear layer. *J. Fluid Mech.* **98** (02), 349–381.

TUTKUN, M., GEORGE, W. K., FOUCAUT, J. M., COUDERT, S., STANISLAS, M. & DELVILLE, J. 2009 In situ calibration of hot wire probes in turbulent flows. *Exp. Fluids* **46** (4), 617–629.

WEI, M. & FREUND, J. 2006 A noise controlled free shear flow. *J. Fluid Mech.* **546**, 123–152.

ZAMAN, K. B. M. Q., BRIDGES, J. E. & HUFF, D. L. 2011 Evolution from tabs to chevron technology – a review. *Intl J. Aeroacoust.* **10** (5), 685–710.

ZHANG, M., JORDAN, P., LEHNASCH, G., CAVALIERI, A. V. G. & AGARWAL, A. 2012 Just enough jitter for jet noise? *AIAA Paper* 2014-3061.

ZHANG, M., TISSOT, G., JORDAN, P., LEHNASCH, G., CAVALIERI, A., COLONIUS, T. & BRES, G. 2015 Non-linear wavepacket forcing for jet noise. In *21st AIAA/CEAS Aeroacoustics Conference Aviation Forum 2015*.

ZHANG, M., TOWNE, A., JORDAN, P., COLONIUS, T., LELE, S. *et al.* 2014 Sound amplification by jittering wavepackets in subsonic turbulent jets. *Bull Am. Phys. Soc.* **59** (20).

https://doi.org/10.1017/jfm.2015.670 Published online by Cambridge University Press